

The effect of shear-thinning behaviour on rod orientation in filled fluids

Julien Férec^{1,†}, Erwan Bertevas², Boo Cheong Khoo², Gilles Ausias¹
and Nhan Phan-Thien²

¹Institut de Recherche Dupuy de Lôme (IRDL), Univ. Bretagne Sud, FRE CNRS 3744, IRDL,
F-56100 Lorient, France

²Department of Mechanical Engineering, National University of Singapore, Singapore 119260, Singapore

(Received 12 October 2015; revised 25 March 2016; accepted 6 May 2016;
first published online 1 June 2016)

In the present article, the cell model (or self-consistent scheme) is used to derive constitutive equations for rod suspensions in non-Newtonian viscous matrices such as power-law, Ellis and Carreau fluids. It is found that the shear-thinning character of the matrix influences considerably the rod contribution to the stress tensor, but has no impact on the rod orientation dynamics: the same microstructure evolution as the one encountered in Newtonian fluids is obtained. The rod suspension behaves differently than the unfilled matrix in the sense that, depending on rod orientation, the onset of shear thinning in the composite occurs at lower or higher shear rates. Our analysis also provides a semi-analytical model for rod suspensions in an Ellis fluid, which appears to be suitable for predicting a Newtonian plateau at low shear rates and a shear-thinning behaviour at high shear rates. In addition, the model predictions are in good agreement with the shear viscosity measurements of glass-fibre-filled polystyrene melts (Chan *et al.*, *J. Rheol.*, vol. 22 (5), 1978, pp. 507–524), demonstrating its ability to describe the rheological behaviour of such polymer composites. Finally, the proposed approach is extended to a Carreau fluid although its solution requires the numerical solution of a set of partial differential equations.

Key words: rheology, slender-body theory, suspensions

1. Introduction

Suspensions of elongated particles in liquids are encountered in several natural and engineered products, with particle size ranging from microscopic (e.g. glass and flax fibres), down to nanoscopic scale (e.g. cellulose nanofibres and carbon nanotubes). Such systems represent an important class of non-Newtonian fluids and therefore, a large body of work in the literature has focused on them. Nevertheless, many unfilled matrices (i.e. molten polymers) exhibit shear-thinning behaviours and the effect of the presence of rods on the composite rheological properties remains unclear.

Composite materials are usually made of polymers which exhibit strong shear-thinning behaviours. Chan, White & Oyanagi (1978) investigated the rheological behaviour of glass-fibre-filled high-density polyethylene and polystyrene melts. It

† Email address for correspondence: julien.ferec@univ-ubs.fr

was reported that both unfilled matrices exhibit shear-thinning behaviour and both glass-fibre-filled systems present viscosity functions of similar form. The viscosity is especially increased by the fibres at low shear rates and the non-Newtonian character of the pure matrix (i.e. shear-thinning behaviour) tends to be enhanced by the glass fibres. These observations have been confirmed by several authors (Czarnecki & White 1980; Kitano & Kataoka 1980; Kitano, Kataoka & Nagatsuka 1984; Becraft & Metzner 1992; Greene & Wilkes 1995; Ramazani, Ait-Kadi & Grmela 2001; Nishitani *et al.* 2007; Ouari *et al.* 2011) and especially for short glass-fibre-filled polypropylene by Mobuchon *et al.* (2005) in shear flows and Férec *et al.* (2009) for extensional flows. Poslinski *et al.* (1988) observed that if a polymeric matrix exhibits Newtonian behaviour at low shear rates and power-law behaviour at high rates of deformation, the addition of solid beads leads to a large increase of the shear viscosity in both regimes, the enhancement being more pronounced in the Newtonian region.

Constitutive equations for fibre-filled systems may generally be written by considering them as two-component fluids, in which the total stress in the composite can be assumed to be (Azaiez 1996)

$$\sigma = -P\delta + \tau^m + \tau^p, \tag{1.1}$$

where P is the isotropic pressure, δ is the identity tensor, τ^m is the matrix contribution and τ^p is the particle contribution to the extra stress tensor. When dealing with a Newtonian medium of viscosity η_0 , the particle contribution to the extra stress tensor, τ^p , takes the following general form up to moderate rod volume concentration ϕ (Hinch & Leal 1975)

$$\tau^p = \eta_0\phi[\mu_1\mathbf{a}_4 : \dot{\gamma} + \mu_2(\dot{\gamma} \cdot \mathbf{a}_2 + \mathbf{a}_2 \cdot \dot{\gamma}) + \mu_3\dot{\gamma} + 2\mu_4\mathbf{a}_2D_r], \tag{1.2}$$

where $\dot{\gamma}$ is the deformation rate tensor and ϕ is the particle volume fraction. $\mathbf{a}_2 = \int_p \mathbf{p}\mathbf{p}\psi \, d\mathbf{p}$ and $\mathbf{a}_4 = \int_p \mathbf{p}\mathbf{p}\mathbf{p}\mathbf{p}\psi \, d\mathbf{p}$ are the second- and fourth-order moments of ψ , the probability distribution function, and $\int_p \dots \psi \, d\mathbf{p}$ refers to an average over all possible rod orientations (Advani & Tucker 1987). \mathbf{a}_2 and \mathbf{a}_4 , the so-called orientation tensors, describe the rod orientation statistics in a representative elementary volume in an efficient and concise way without a significant loss of information. The coefficients (μ_i , $i = 1, 2, 3, 4$) in (1.2) are geometric shape factors (see the table in Férec & Ausias 2015), and D_r is the rotary diffusivity due to Brownian motion. For slender rods, particle thickness can be ignored and this is achieved by setting μ_2 and μ_3 equal to zero. If the particle is large enough so that Brownian motion can be ignored, the last term containing D_r can be omitted. Three regimes of rod concentrations are proposed in the literature according to particle shape (Doi & Edwards 1986): dilute, for which $\phi < 1/a_r^2$; semi-dilute when $1/a_r^2 < \phi < 1/a_r$ and concentrated for $1/a_r < \phi$, where $a_r = L/D$ is the particle aspect ratio, L and D being its length and diameter, respectively.

The creeping flow equations were solved by Jeffery (1922) for a rigid ellipsoid freely suspended in a Newtonian fluid assuming a linearly varying flow and it was found that the centre of the particle translates with the local fluid velocity. Furthermore, the particle orientation is described by a unit vector \mathbf{p} directed along its principal axis, and Jeffery (1922) showed that

$$\frac{D\mathbf{p}}{Dt} = -\frac{1}{2}\boldsymbol{\omega} \cdot \mathbf{p} + \frac{\lambda}{2}(\dot{\gamma} \cdot \mathbf{p} - \dot{\gamma} : \mathbf{p}\mathbf{p}\mathbf{p}) - \frac{C_I|\dot{\gamma}|}{\psi} \frac{\partial\psi}{\partial\mathbf{p}}, \tag{1.3}$$

where D/Dt denotes the material derivative and $\boldsymbol{\omega}$ is the vorticity tensor (see Bird, Armstrong & Hassager 1987a for its definition). The shape factor defined by $\lambda = (a_r^2 - 1)/(a_r^2 + 1)$ equals unity for a slender body ($a_r \rightarrow \infty$). The last term on the right-hand side of (1.3) was later introduced by Folgar & Tucker (1984) to take into account particle interactions. In their theory, $|\dot{\gamma}|$ is the effective deformation rate (equal to the shear rate in simple shear) and C_I is a hydrodynamic diffusion coefficient. Bay (1991) and Phan-Thien *et al.* (2002) have related C_I to rod volume fraction, ϕ , and particle aspect ratio, a_r . Following (1.3), Advani & Tucker (1990) derived the time evolution for the second-order orientation tensor, \mathbf{a}_2 and obtained

$$\frac{D\mathbf{a}_2}{Dt} = -\frac{1}{2}(\boldsymbol{\omega} \cdot \mathbf{a}_2 - \mathbf{a}_2 \cdot \boldsymbol{\omega}) + \frac{\lambda}{2}(\dot{\gamma} \cdot \mathbf{a}_2 + \mathbf{a}_2 \cdot \dot{\gamma} - 2\mathbf{a}_4 : \dot{\gamma}) + 2C_I|\dot{\gamma}|(\boldsymbol{\delta} - 3\mathbf{a}_2). \quad (1.4)$$

Equation (1.4) represents the orientation dynamics for a rod population suspended in a Newtonian fluid and required closure approximations to evaluate \mathbf{a}_4 , the fourth-order orientation tensor (Advani & Tucker 1990; Cintra & Tucker 1995; Dupret & Verleye 1999; Sepehr *et al.* 2004). The first two terms (in brackets) on the right-hand side of (1.4) stand for the hydrodynamic contribution whereas the last part is related to diffusion due to particle interactions. The dimensionless form of (1.4) (convection–diffusion type) involves definition of a Péclet number such as $P_e = 1/C_I$, which controls the steady-state orientation for the rods (i.e. low P_e refers to random orientation whereas high P_e suggests rod alignment towards the flow direction in simple shear flow).

The above mentioned constitutive equations do not account for the shear-thinning character of the unfilled matrices, but some developments were proposed in order to provide more realistic models and understand flow phenomena in composite processing. Early attempts simply replaced the Newtonian viscosity in (1.2) by that of the polymer $\eta_0 = \eta^m(\dot{\gamma})$ which is shear-rate dependent, the equation of change for \mathbf{a}_2 , equation (1.4), being left unchanged. Azaiez (1996) developed constitutive equations for fibre suspensions in polymer solutions based on the FENE-P (Finitely Extensible Nonlinear Elastic – Peterlin), FENE-CR (Finitely Extensible Non-linear Elastic – Chilcott and Rallison) and Giesekus models. A parameter was also introduced to couple the effects of fibre orientation with the hydrodynamic drag acting on the beads composing the dumbbells. For steady-state shear flow, Azaiez (1996) reported a strong shear-thinning character in the coupled case for the three rheological models although the FENE-CR model with the uncoupled case exhibits a constant steady-state viscosity. Ait-Kadi & Grmela (1994) used the generalized Poisson bracket formalism and their choice for the Helmholtz free energy function yielded a FENE-P type matrix. In the case of the steady shear flow, their results showed that the presence of fibres results in an increase of both the viscosity and the first normal stress coefficient over the whole range of shear rates. Ramazani and coauthors (Ramazani, Ait-Kadi & Grmela 1997; Ramazani *et al.* 2001) extended this work by introducing anisotropic expressions for the mobility tensor in an attempt to capture fibre-matrix interactions. Rajabian, Dubois & Grmela (2005) adopted a similar approach to account for fibre flexibility and observed that the steady-state relative viscosity increases with fibre flexibility, especially in the shear-thinning region. Beaulne & Mitsoulis (2003) used the K-BKZ integral constitutive equation which described the experimental results of Greene & Wilkes (1995) fairly well. Note that some authors (Kagarise *et al.* 2010, 2011) also used the multi-mode Giesekus model to predict the strain-rate-dependent behaviour of the polymer matrix.

In a second type of attempt, cell models (or self-consistent schemes) were used to derive more realistic constitutive equations than those cited previously. This was initiated with the seminal work of Batchelor (1971), who theoretically analysed the elongational flow of a Newtonian fluid filament around a rod parallel to the flow direction and contained in a cell. The same problem was then extended by Goddard (1976a,b) to include the strain-thinning behaviour of the matrix by considering a power-law model. Both authors attributed the viscous resistance of elongational flow to the shearing of the fluid between parallel suspended fibres. In the case of shear-thinning fluids, Goddard (1978) found that the particle influence on the extensional flow as well as on the particle contribution to bulk stress are both greatly diminished as compared to the Newtonian case, and the quantitative agreement with some experimental data is discussed in White & Czarnecki (1980). Dinh & Armstrong (1984) also used the Batchelor approach to develop a rheological equation of state to describe non-dilute suspensions of fibres in Newtonian solvents undergoing homogeneous extensional and shear flows. This work was then extended by Wang & Cheau (1991) who proposed a constitutive model for semi-concentrated suspensions of rigid fibres in an Ellis fluid. However, in their model derivation, it was assumed that the outer boundary condition for the axial velocity is $\dot{\gamma}D/2$ ($\dot{\gamma}$ and $D/2$ being respectively the shear rate and particle radius), which appears to be unphysical. In addition, Wang & Cheau (1991) did not take into account the dependency of particle orientation on the axial velocity. Souloumiac & Vincent (1998) improved the original work of Batchelor (1971) and Goddard (1976a) by considering rod orientation and their result is applicable to homogeneous flow, especially to shear flow. Souloumiac & Vincent (1998) established a stress expression which includes the shear-thinning behaviour of the matrix as represented by a power law and given by

$$\tau^p = K\phi\mu_1^{(m)}\dot{\gamma} : \int_p pppp|\dot{\gamma} : pp|^{m-1}\psi dp, \quad (1.5)$$

where K is the matrix consistency (Pa s^m) and m is the power-law index of the matrix which was found by Souloumiac & Vincent (1998) to be the same for the suspension as for the unfilled matrix. The dimensionless coupling coefficient $\mu_1^{(m)}$ is given by

$$\mu_1^{(m)} = \frac{\alpha_r^{m+1}}{2^{m-1}(m+2)} \left[\frac{1-m}{m[1-(D/2h)^{(1-m)/m}]} \right]^m. \quad (1.6)$$

If m tends to 1, equation (1.6) reduces to the expression proposed by Dinh & Armstrong (1984). Gibson & Toll (1999) developed a non-local relationship for the stress generated in a planar suspension of rods where the local interactions are governed by a power-law drag law. Note that indeed, most equations for rod suspensions given in the literature are local, i.e. the stress at a material point depends only on the rate of deformation at that same point. For homogeneous flows of statistically homogeneous suspensions, their expression reduces to (1.5). In order to reproduce a Newtonian plateau at low strain rates and a strain-thinning behaviour at high strain rates, Férec *et al.* (2009) later proposed an empirical extension of the Carreau model for suspended fibres in a polymeric fluid. As a final remark, it is also important to note that none of the above theories aimed at tackling the description of rod dynamics in such shear-thinning non-Newtonian fluids.

The purpose of this paper is firstly to revisit the cell model in order to derive in details a constitutive equation for rod suspensions in fluids which exhibit a

Newtonian plateau at low shear rates and a shear-thinning behaviour at high shear rates. Our approach is validated, step by step, by recovering established results for Newtonian and power-law unfilled matrices. Based on these results, the effect of shear-thinning behaviour on rod orientation in filled systems is investigated: what is the enhancement/decrease of the suspension shear viscosity in a power-law matrix as compared to the Newtonian one? Does the onset of non-Newtonian behaviour occur at the same characteristic time (shear rate) for unfilled and filled systems? These are some of the questions we wish to address. Particular aspects of rod orientation in such shear-thinning matrices are also discussed. Finally, the present self-consistent approach is extended to formulate a constitutive equation describing the rheological properties of semi-concentrated suspensions of rigid rods in Ellis and Carreau fluids. In addition, the model predictions for an Ellis fluid are shown to be in good agreement with rheological data for glass-fibre-filled polystyrene melts (Chan *et al.* 1978), demonstrating its ability to describe the shear viscosities of rod/polymer composites.

2. Cell model revisited

The rod (referred to throughout the article as rod, particle or fibre) is represented by a straight cylinder of length L having a circular cross-section of radius R (or equivalently of diameter D) and is considered to be a slender body. Its aspect ratio, defined by $a_r = L/D \gg 1$, enables us to neglect the particle end effects.

2.1. Cell model

The test rod is coaxially embedded into a cylindrical fluid cell of radius h and of the same length as the particle (figure 1). This cell model assumes that the effect of one fibre on its neighbours is approximated by an equivalent cylindrical boundary around the test rod, and therefore simplifies the problem to a single-particle theory. In order to determine the velocity field near a slender particle, a dimensional analysis is carried out using a cylindrical coordinate system for convenience. First, the fluid velocity field is considered in the vicinity ($|z| < L/2$ and $r \ll L/2$) of a particle in the assumed equilibrium orientation, as shown schematically in figure 1. Provided that the cross-sectional form of the particle is circular and does not vary with the axial z -position, it is useful to adopt a dimensional scaling for the velocities and the velocity gradients. Thus, the dimensionless quantities are distinguished by asterisks such as

$$r = Rr^*, \quad \theta = \theta^*, \quad z = \frac{L}{2}z^* \quad \text{and} \quad u_r = R|\dot{\gamma}|u_r^*, \quad u_\theta = R|\dot{\gamma}|u_\theta^*, \quad u_z = \frac{L}{2}|\dot{\gamma}|u_z^*. \quad (2.1a,b)$$

We are concerned with the limiting forms of the dimensionless velocities u_r^* , u_θ^* and u_z^* and their r^* , θ^* , z^* -derivatives for $a_r \rightarrow \infty$ in an inner region near the body, where r^* , θ^* and z^* are all $O(1)$. Since the gradient operator is given by

$$\nabla = \delta_r \frac{\partial}{\partial r} + \delta_\theta \frac{1}{r} \frac{\partial}{\partial \theta} + \delta_z \frac{\partial}{\partial z} = \frac{1}{R} \left(\nabla^{(0)} + \frac{1}{a_r} \nabla^{(1)} \right), \quad (2.2)$$

where

$$\nabla^{(0)} = \delta_r \frac{\partial}{\partial r^*} + \delta_\theta \frac{1}{r^*} \frac{\partial}{\partial \theta^*} \quad \text{and} \quad \nabla^{(1)} = \delta_z \frac{\partial}{\partial z^*}, \quad (2.3a,b)$$

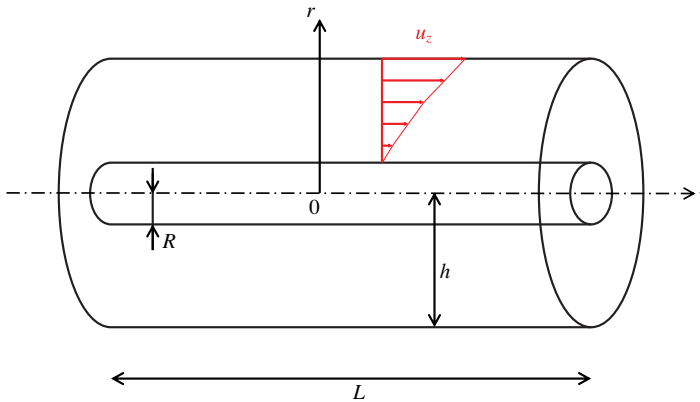


FIGURE 1. (Colour online) Geometry of the cell surrounding the test rod.

one has formally for the velocity gradient

$$\nabla \mathbf{u} = a_r |\dot{\gamma}| [\nabla^{(0)} (\delta_z u_z^*)] = a_r |\dot{\gamma}| \left[\delta_r \delta_z \frac{\partial u_z^*}{\partial r^*} + O(u/a_r) \right], \tag{2.4}$$

where the θ^* -derivatives have been omitted due to the problem symmetry. Here, we denote by $O(u/a_r)$ the terms which are $O(1/a_r)$ relative to the leading terms in (2.4). The leading terms themselves suggest that a quasi-steady and shear-dominated flow occurs in the near field, which implies the validity of a viscometric flow representation for the fluid rheology (Batchelor 1971; Goddard 1976a,b). Therefore, this cell model provides a useful approximation in the particle near field, with constant velocity gradients along the rod.

For this axisymmetric problem, the axial velocity u_z satisfies the following equation of motion in terms of stress in cylindrical coordinates

$$\frac{1}{r} \frac{\partial}{\partial r} (r \tau_{rz}) = 0, \tag{2.5}$$

where τ_{rz} represents the shear stress. First, equation (2.5) can be integrated directly to give the familiar elementary form for the shear stress $\tau_{rz} = \tau_R R/r$, where τ_R is the unknown stress at the rod surface (a no-slip condition is considered at the particle surface). Secondly, it is assumed that the rheological relationship can be inverted to give the shear rate, $\dot{\gamma}$, as a function of the shear stress. Hence, following a change of variable (i.e. $r = R \tau_R / \tau_{rz}$), the axial velocity u_z can be expressed as

$$u_z = \int_R^r \dot{\gamma} \, dr = \tau_R R \int_{\tau_R R/r}^{\tau_R} \frac{\dot{\gamma}}{\tau_{rz}^2} \, d\tau_{rz}. \tag{2.6}$$

Once the shear rheology of the fluid is known, this result provides a relationship between the axial velocity distribution and the rod surface stress τ_R . At the same time, it becomes evident that an outer boundary condition is required to determine τ_R . At $r = h$, the relative fluid velocity field is assumed to be undisturbed by the particle. For an inertialess particle, a force balance shows that its centre of mass translates affinely with the bulk flow. Hence, the fluid velocity at distance $z\mathbf{p}$ from the centre of mass of

the rod is $\mathbf{u}^{fluid} = z\boldsymbol{\kappa} \cdot \mathbf{p}$, where $\boldsymbol{\kappa}$ is the transpose of the velocity gradient tensor (Bird *et al.* 1987a), whereas the rod velocity at the same location is $\mathbf{u}^{rod} = z\dot{\mathbf{p}}$. The relative velocity is $\mathbf{u} = \mathbf{u}^{fluid} - \mathbf{u}^{rod}$, and hence its component along the z -direction, is found to be $\mathbf{u} \cdot \mathbf{p} = z\boldsymbol{\kappa} : \mathbf{pp}$, which gives the condition $u_z(h) = z\dot{\boldsymbol{\gamma}} : \mathbf{pp}/2$ (when expressed in the local coordinate system). z is the arc length measured along the rod axis of direction \mathbf{p} with $z = 0$ at the centre of the rod (figure 1). With this result in mind, equation (2.6) yields

$$z\dot{\boldsymbol{\gamma}} : \mathbf{pp}/2 = \tau_R R \int_{\tau_R R/h}^{\tau_R} \frac{\dot{\boldsymbol{\gamma}}}{\tau_{rz}^2} d\tau_{rz}. \quad (2.7)$$

Note that $\dot{\boldsymbol{\gamma}}$ is the unperturbed deformation rate tensor taken at the outer boundary of the cell and $\dot{\boldsymbol{\gamma}} = \partial u_z / \partial r$ is the disturbed shear rate close to the rod. Equation (2.7) is a key formula used throughout this article in order to take into account the contribution of particles suspended in nonlinear matrices. An elementary force balance on the particle leads to the force per unit length $f = 2\pi R \tau_R$. This axial tensile force is parallel to the unit vector \mathbf{p} , as Batchelor (1971) argued that the components normal to the particle make no contribution in the case of a rod on which no external force or couple acts.

The average force carried by the rod is then substituted into the Kramer expression (Bird *et al.* 1987b) to derive the rod stress tensor, in which the volume fraction of particles, ϕ , takes into account the contribution of each particle contained in a given volume. Hence, the extra stress due to the particle contribution is

$$\boldsymbol{\tau}^p = \frac{2\phi}{\pi R^2 L} \left\langle \mathbf{pp} \int_{z=0}^{z=L/2} z f dz \right\rangle, \quad (2.8)$$

where the angular brackets denote the ensemble average with respect to the distribution function of \mathbf{p} . Equation (2.8) shows that the stress can be directly computed once the drag force is known.

2.2. Results for Newtonian fluids

If a Newtonian medium of viscosity η_0 is considered, the usual rheological constitutive equation expressed in simple shear flow is $\dot{\boldsymbol{\gamma}} = \tau_{rz}/\eta_0$ and (2.7) becomes

$$f = \frac{\pi \eta_0}{\log(h/R)} z \dot{\boldsymbol{\gamma}} : \mathbf{pp}, \quad (2.9)$$

which is the well-known parallel drag force for a rod suspended into a Newtonian fluid. Combining (2.8) and (2.9) leads to the following particle contribution to the stress tensor

$$\boldsymbol{\tau}^p = \eta_0 \phi \frac{a_r^2}{3 \log(h/R)} \dot{\boldsymbol{\gamma}} : \langle \mathbf{pppp} \rangle. \quad (2.10)$$

In order to derive the evolution equation for the second-order tensor $\langle \mathbf{pp} \rangle$, Giesekus (1962) proposed an ingenious method to determine the stress tensor (which is frequently used in the kinetic theory of polymer solutions and melts (Bird *et al.* 1987b)) and is referred to as the Giesekus stress tensor. This result can be used to derive the extra stress due to the particle contribution and is given by

$$\boldsymbol{\tau}^p = -\frac{n\zeta}{4} \frac{\mathcal{D}\langle \mathbf{pp} \rangle}{\mathcal{D}t}, \quad (2.11)$$

where n represents the number of particles per unit volume. In order to define this derivative, we remark that the Giesekus formulation involves a convected derivative of the contravariant components of a second-order tensor, Δ , defined by

$$\frac{\mathcal{D}\Delta}{\mathcal{D}t} = \frac{D\Delta}{Dt} + \frac{1}{2}(\omega \cdot \Delta - \Delta \cdot \omega) - \frac{1}{2}(\dot{\gamma} \cdot \Delta + \Delta \cdot \dot{\gamma}). \tag{2.12}$$

A comparison of (2.10) and (2.11) with the help of (2.12) leads to

$$\frac{D\langle pp \rangle}{Dt} = -\frac{1}{2}(\omega \cdot \langle pp \rangle - \langle pp \rangle \cdot \omega) + \frac{1}{2}(\dot{\gamma} \cdot \langle pp \rangle + \langle pp \rangle \cdot \dot{\gamma} - 2\dot{\gamma} : \langle pppp \rangle), \tag{2.13}$$

and the drag coefficient is found to be

$$\zeta = \frac{\eta_0 \pi L^3}{3 \log(h/R)}. \tag{2.14}$$

These last results are in agreement with those obtained by Dinh & Armstrong (1984) for semi-concentrated fibre suspensions in Newtonian fluids. Hence, a rheological constitutive equation for slender rods in Newtonian fluids can be expressed as follows

$$\sigma = -P\delta + \eta_0 \dot{\gamma} + \eta_0 \phi \frac{a_r^2}{3 \log(h/R)} \dot{\gamma} : \langle pppp \rangle. \tag{2.15}$$

3. Power-law fluids

3.1. Constitutive equation for suspensions in power-law fluids

For power-law fluids, the shear-rate versus shear-stress rheological relation can be written as $\dot{\gamma} = \tau_{rz}/K|\tau_{rz}/K|^{(1-m)/m}$. The latter expression is substituting in (2.7) to give the following drag force

$$f = \frac{\pi K}{(2R)^{m-1}} \left[\frac{1-m}{m[1-(R/h)^{(1-m)/m}]} \right]^m z^m |\dot{\gamma} : pp|^{m-1} \dot{\gamma} : pp. \tag{3.1}$$

It is interesting to note the nonlinear dependency of the drag force on the magnitude of the strain-rate tensor and the particle orientation through the dyadic product of p . This expression is then inserted in (2.8) and an analytical integration along the arc length can be performed to result in

$$\tau^p = K\phi \frac{a_r^{m+1}}{2^{m-1}(m+2)} \left[\frac{1-m}{m[1-(R/h)^{(1-m)/m}]} \right]^m \dot{\gamma} : \langle |\dot{\gamma} : pp|^{m-1} pppp \rangle, \tag{3.2}$$

which is exactly the stress contribution for rod suspensions in power-law fluids obtained by Souloumiac & Vincent (1998) and Gibson & Toll (1999). In the special case of $m = 1$, the solution reduces to (2.10) with $K = \eta_0$. Examination of (3.2) reveals that the slope of $\log \tau_{12}^p$ versus $\log \dot{\gamma}$, where τ_{12}^p is the particle shear stress, is given by the exponent of m , which is the same slope as the suspending fluid: the model predicts that the presence of rods does not alter the slope with which the suspension shear thins. A rheological constitutive equation for axisymmetric particles in power-law fluids can then be represented as follows

$$\sigma = -P\delta + K|\dot{\gamma}|^{m-1} \dot{\gamma} + K\phi \frac{a_r^{m+1}}{2^{m-1}(m+2)} \left[\frac{1-m}{m[1-(R/h)^{(1-m)/m}]} \right]^m \dot{\gamma} : \langle |\dot{\gamma} : pp|^{m-1} pppp \rangle. \tag{3.3}$$

To derive the time evolution equation for the rod microstructure, the Giesekus expression is used again and yields to the following expression

$$\begin{aligned} \frac{D\langle |\dot{\boldsymbol{\gamma}} : \boldsymbol{pp}|^{m-1} \boldsymbol{pp} \rangle}{Dt} = & -\frac{1}{2}(\boldsymbol{\omega} \cdot \langle |\dot{\boldsymbol{\gamma}} : \boldsymbol{pp}|^{m-1} \boldsymbol{pp} \rangle - \langle |\dot{\boldsymbol{\gamma}} : \boldsymbol{pp}|^{m-1} \boldsymbol{pp} \rangle \cdot \boldsymbol{\omega}) \\ & + \frac{1}{2}(\dot{\boldsymbol{\gamma}} \cdot \langle |\dot{\boldsymbol{\gamma}} : \boldsymbol{pp}|^{m-1} \boldsymbol{pp} \rangle + \langle |\dot{\boldsymbol{\gamma}} : \boldsymbol{pp}|^{m-1} \boldsymbol{pp} \rangle \cdot \dot{\boldsymbol{\gamma}} \\ & - 2\dot{\boldsymbol{\gamma}} : \langle |\dot{\boldsymbol{\gamma}} : \boldsymbol{pp}|^{m-1} \boldsymbol{pppp} \rangle), \end{aligned} \quad (3.4)$$

where $\langle |\dot{\boldsymbol{\gamma}} : \boldsymbol{pp}|^{m-1} \boldsymbol{pp} \rangle$ is a symmetric second-order tensor. In order to gain insight into the orientation evolution of a rod, the time evolution equation for the probability distribution function, assuming the existence of a diffusive contribution as suggested by Folgar & Tucker (1984), is given by

$$\frac{D\psi}{Dt} = -\frac{\partial}{\partial \boldsymbol{p}} \cdot (\dot{\boldsymbol{p}}\psi) + C_I |\dot{\boldsymbol{\gamma}}| \frac{\partial^2 \psi}{\partial \boldsymbol{p}^2}, \quad (3.5)$$

where $\partial/\partial \boldsymbol{p}$ is the differential operator on the surface of a unit sphere. $\dot{\boldsymbol{p}}$ remains to be expressed considering that the suspending fluid follows a power-law behaviour. Hence, it is assumed at this point that $\dot{\boldsymbol{p}}$ is given by the Jeffery equation (1.3) for a slender body (i.e. $\lambda = 1$) with no diffusion (i.e. $C_I = 0$). Although Jeffery (1922) solved the velocity field around a single rigid ellipsoidal particle immersed in a Newtonian fluid with negligible inertia, this assumption is justified as for a single material point in simple shear flow, the Newtonian viscosity of the surrounding fluid can be replaced by a local viscosity predicted by the power-law model (still a viscous fluid with no time dependence and no normal stress differences). This assumption appears to be all the more valid since the viscosity term does not appear in the Jeffery solution. In our cell model, the velocity gradient is also assumed constant along the length of the particle. Moreover, a force balance using (3.1) leads to the rod centroid moving affinely with regards to the effective medium in the absence of any other forces besides those imparted by the suspending fluid, as also suggested by Jeffery (1922). Thus the Jeffery equation is substituted into (3.5) and the convective part for the time evolution of $\langle |\dot{\boldsymbol{\gamma}} : \boldsymbol{pp}|^{m-1} \boldsymbol{pp} \rangle$ is found to be (3.4) (details on the derivation are given in appendix A). We were unfortunately unable to straightforwardly express the time evolution for the diffusive term.

Dividing (3.4) by $\langle |\dot{\boldsymbol{\gamma}} : \boldsymbol{pp}|^{m-1} \rangle$, which corresponds to the trace of $\langle |\dot{\boldsymbol{\gamma}} : \boldsymbol{pp}|^{m-1} \boldsymbol{pp} \rangle$, equation (3.4) results in

$$\frac{D\boldsymbol{a}_2^{(m)}}{Dt} = -\frac{1}{2}(\boldsymbol{\omega} \cdot \boldsymbol{a}_2^{(m)} - \boldsymbol{a}_2^{(m)} \cdot \boldsymbol{\omega}) + \frac{1}{2}(\dot{\boldsymbol{\gamma}} \cdot \boldsymbol{a}_2^{(m)} + \boldsymbol{a}_2^{(m)} \cdot \dot{\boldsymbol{\gamma}} - 2\dot{\boldsymbol{\gamma}} : \boldsymbol{a}_4^{(m)}), \quad (3.6)$$

where $\boldsymbol{a}_2^{(m)} = \langle |\dot{\boldsymbol{\gamma}} : \boldsymbol{pp}|^{m-1} \boldsymbol{pp} \rangle / \langle |\dot{\boldsymbol{\gamma}} : \boldsymbol{pp}|^{m-1} \rangle$ and $\boldsymbol{a}_4^{(m)} = \langle |\dot{\boldsymbol{\gamma}} : \boldsymbol{pp}|^{m-1} \boldsymbol{pppp} \rangle / \langle |\dot{\boldsymbol{\gamma}} : \boldsymbol{pp}|^{m-1} \rangle$ have been used. Similarly to the orientation tensors (Advani & Tucker 1987), $\boldsymbol{a}_2^{(m)}$ and $\boldsymbol{a}_4^{(m)}$ describe an equivalent orientation state for the rods, for which the drift due to the scalar potential $|\dot{\boldsymbol{\gamma}} : \boldsymbol{pp}|^{m-1}$ is considered (note that the trace of $\boldsymbol{a}_2^{(m)}$ always equals 1).

Equation (3.6) is structured as (1.4) which is expressed for a Newtonian matrix with infinite particle aspect ratio ($\lambda = 1$) and no diffusion ($C_I = 0$). Therefore, these compact and efficient tensors are also called orientation tensors. The components of the second-order orientation tensor have some simple physical interpretations. If all

its diagonal components are $1/3$, the orientation tensor indicates a three-dimensional isotropic orientation state for the rods. When two diagonal components are equal to $1/2$, the tensor implies a two-dimensional random, planar bi-axial or planar orientation. Finally, a perfect uniaxial alignment results in one diagonal component value of 1 .

The previous governing equations (3.3) and (3.4) are not satisfactory to completely close the problem: one needs some approximations such as closure relations. The objective of this work is not to focus on the development of such relations and the accompanying issue of questionable accuracy. Therefore, equation (3.6) will no longer be used in the rest of the paper and the results presented hereafter will be based on the numerical solution of the Fokker–Planck equation (3.5) with $C_I \neq 0$, where $\dot{\mathbf{p}}$ is given by the Jeffery equation for slender bodies and a description of the numerical method is detailed in Férec *et al.* (2008). Hence, once the probability distribution function is numerically computed, the components of $\mathbf{a}_2^{(m)}$ and $\mathbf{a}_4^{(m)}$ are straightforwardly evaluated and the stress tensor components obtained.

3.2. Model predictions

In order to investigate the model predictions, a first set of simulations was performed imposing a fixed isotropic orientation distribution (i.e. $\psi = 1/4\pi$). All the results presented in this section are obtained for the following parameters: $K = 50$ Pa s^m , $\phi = 10\%$, $a_r = 20$ ($L = 280$ μm and $R = 14$ μm) and $h = D\sqrt{\pi/4\phi}$ (Chung & Kwon 1996). This last parameter corresponds to the average distance between rods for an aligned orientation state (Dinh & Armstrong 1984) and is kept constant over the different simulations even if the particle microstructure orientation evolves.

A steady-state shear flow is considered (the imposed shear rate is 1 s^{-1}), where subscripts 1, 2 and 3 stand for flow, velocity gradient and vorticity directions, respectively. Assuming an isotropic rod orientation distribution ($\psi = 1/4\pi$), figure 2 reports the particle shear-stress contribution, τ_{12}^p , and the non-zero components of $\mathbf{a}_2^{(m)}$ as functions of m . τ_{12}^p exhibits a decrease with increasing shear-thinning character of the matrix (i.e. m decreases). Starting from an isotropic effective rod orientation $\mathbf{a}_2^{(m)}$ for $m = 1$, observation of $\mathbf{a}_2^{(m)}$ reveals that the enhancement of the shear-thinning character of the matrix results in a system which behaves effectively like a suspension in which more and more rods would orient towards the vorticity axis: $a_{33}^{(m)}$ tends to 1 whereas $a_{22}^{(m)}$ and $a_{11}^{(m)}$ decrease to 0. Therefore, the effect of the scalar $|\dot{\boldsymbol{\gamma}} : \mathbf{pp}|^{m-1}$ is similar to a stretching force on the orientation distribution in the 3-direction as $a_{11}^{(m)}$ remains equal to $a_{22}^{(m)}$.

The transient results are not shown here as the orientation states predicted by (3.5) are similar to the ones considering a Newtonian matrix and are well known (Férec *et al.* 2008). Note also that the influence of the rod aspect ratio and the particle concentration on the coupling coefficient, $\mu_1^{(m)}$, have already been tested in Souloumiac & Vincent (1998).

3.3. Newtonian versus power-law fluids

Regarding the stress expressions for the rod-filled systems in both Newtonian (2.10) and power-law (3.2) matrices, some questions dealing with the enhancement/decrease of the suspension shear viscosity in a power-law matrix and the departure from Newtonian behaviour arise. In order to provide some answers, the specific shear viscosities of the suspensions ($\eta_{sp} = (\eta/\eta^m) - 1$, where η and η^m are the shear

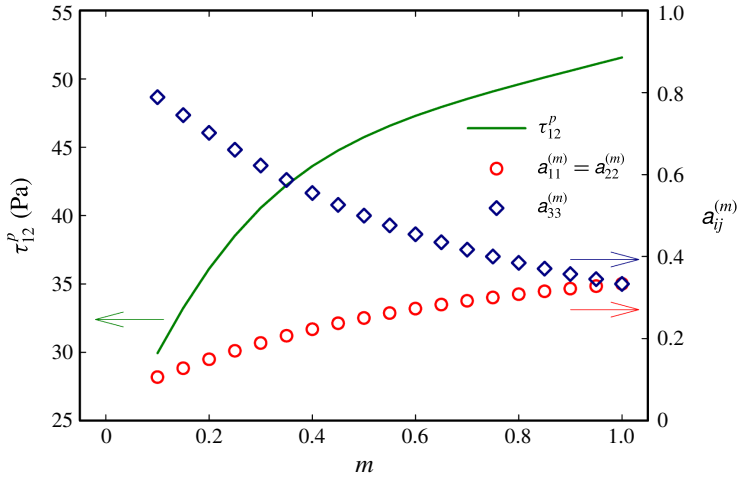


FIGURE 2. (Colour online) Effect of the power-law index, m , on the shear stress τ_{12}^p and on the non-zero components of $\mathbf{a}_2^{(m)}$.

viscosities for the composite and the unfilled matrix, respectively) in both Newtonian and pseudo-plastic matrices are given respectively by

$$\eta_{sp}^N = \phi \frac{2\alpha_r^2}{3 \log(h/R)} \langle p_1 p_1 p_2 p_2 \rangle, \tag{3.7}$$

and

$$\eta_{sp}^{PL} = \phi \frac{2\alpha_r^{m+1}}{2^{m-1}(m+2)} \left[\frac{1-m}{m[1-(R/h)^{(1-m)/m}]} \right]^m \langle |\tilde{\boldsymbol{\gamma}} : \mathbf{pp}|^{m-1} p_1 p_1 p_2 p_2 \rangle, \tag{3.8}$$

where $\tilde{\boldsymbol{\gamma}}$ is the dimensionless strain-rate tensor. The quantities $\langle p_1 p_1 p_2 p_2 \rangle$ and $\langle |\tilde{\boldsymbol{\gamma}} : \mathbf{pp}|^{m-1} p_1 p_1 p_2 p_2 \rangle$ are calculated from steady-state solutions of (3.5).

Figure 3 reports the Newtonian specific viscosity, η_{sp}^N , as a function of Péclet number ($P_e = 1/C_I$), as well as η_{sp}^{PL} for $m = 0.6$ and 0.3 , respectively (note that C_I in (3.5) controls the diffusion due to rod interactions). Starting with an isotropic rod orientation state ($P_e \ll 1$), the specific viscosity decreases with diminishing the power-law index, the largest value being observed for the suspension in a Newtonian fluid. In the region of $P_e \approx 10$, the isotropic orientation distribution of the rods is destroyed and the resulting microstructure leads to systems having the most flow resistance. For Newtonian fluids, the maximum is reached for a configuration in which the largest number of rods is in close alignment with the principal axis of strain. At larger P_e , decrease in viscosity due to rod orientation is observed and is more pronounced as m becomes close to 1: rods orient toward directions in which the energy dissipation is the lowest. Finally at $P_e > 10^3$, the specific viscosity for the most shear-thinning matrix (i.e. $m = 0.3$) becomes the highest.

In order to explain this behaviour, the $a_{11}^{(m)}$ and $a_{33}^{(m)}$ components of the second-order orientation tensor are depicted as functions of P_e for the three different fluids in figure 4. As previously mentioned, considering an isotropic orientation state (i.e. $\psi = \text{const.}$) for rods suspended in shear-thinning fluids (i.e. $m \neq 1$) leads to

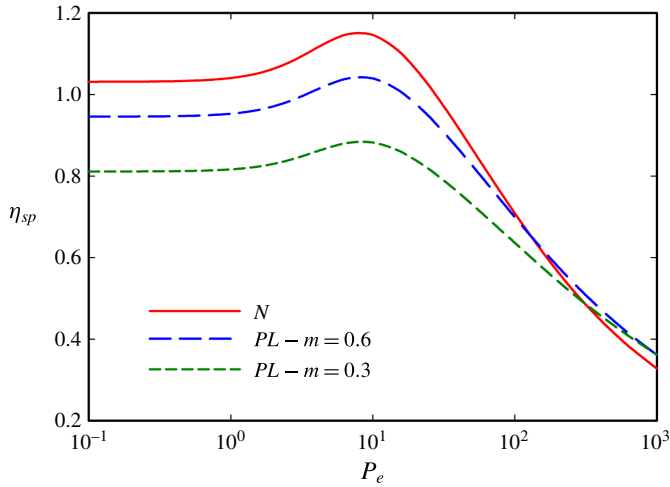


FIGURE 3. (Colour online) Specific viscosities for rod suspensions in a Newtonian fluid (N) and two power-law fluids with $m = 0.6$ and 0.3 , respectively.

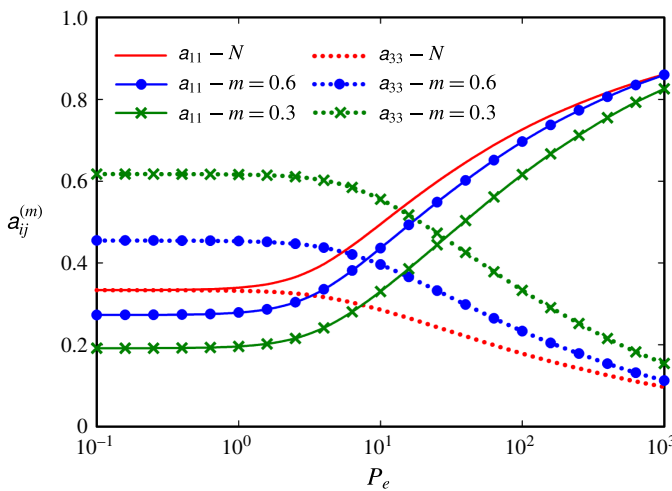


FIGURE 4. (Colour online) $a_{11}^{(m)}$ and $a_{33}^{(m)}$ as a function of P_e for a Newtonian (N) and two shear-thinning ($m = 0.6$ and 0.3) fluids, respectively.

$a_{11}^{(m)} \neq a_{33}^{(m)} \neq 1/3$. At large P_e and independently of m , $a_{11}^{(m)}$ and $a_{33}^{(m)}$ tend to reach the same steady-state values close to 0.9 and 0.1 , respectively. These results suggest that the shear-thinning behaviour of the matrix has no effect on the rod orientation dynamics in the case of strong flows. For $P_e \rightarrow \infty$, the steady-state solution for the distribution function is simply a Dirac function that is $\psi(\mathbf{p}) = \delta(\mathbf{p} - \delta_1)$, where the subscript 1 stands for the flow direction. Under these conditions, the steady-state shear viscosity for the suspension is equal to the unfilled viscosity because of the alignment of the rods in the planes of shear and the lack of inclusion of rod thickness in the model. Hence, as $P_e \rightarrow \infty$, the specific viscosities converge to zero and all the components of $\mathbf{a}_2^{(m)}$ are null, except $a_{11}^{(m)}$, which is 1 .

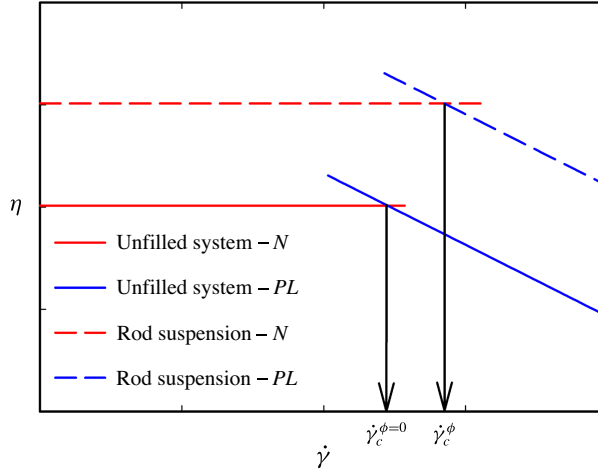


FIGURE 5. (Colour online) Diagram defining the critical shear rates, $\dot{\gamma}_c^\phi$ and $\dot{\gamma}_c^{\phi=0}$.

4. Nonlinear viscous fluids

In view of this, we first consider a model in which an inelastic fluid whose shear viscosity dependency on shear rate is described by a combination of Newtonian and power-law models, as illustrated in figure 5. Note that such materials are usually referred to as bi-viscous fluids. The Ellis and Carreau models are then considered as potential candidates to overcome the shortcomings of the power-law model and the present approach is applied to both these models below.

4.1. Bi-viscous model

To investigate the departure from the plateau region, the rod contribution to the stress in the suspension is assumed to follow the Newtonian behaviour predicted by (2.15) at low shear rates and the power-law form given by (3.3) at high shear rates. The transition behaviour at intermediate shear rates is not necessary. Therefore, equating the shear viscosities of the suspension in both these limiting regions enables defining a critical shear rate $\dot{\gamma}_c^\phi$ at which the transition occurs from the zero-shear-rate plateau to the power-law regime (figure 5). After some straightforward calculus, the critical shear rate of the suspension is given by

$$\dot{\gamma}_c^\phi = \left[\frac{\eta_0 + \eta_0\phi \frac{2a_r^2}{3 \log(h/R)} \langle p_1 p_1 p_2 p_2 \rangle}{K + K\phi \frac{2a_r^{m+1}}{2^{m-1}(m+2)} \left(\frac{1-m}{m[1-(R/h)^{(1-m)/m}]} \right)^m \langle |\tilde{\mathbf{Y}} : \mathbf{p}\mathbf{p}|^{m-1} p_1 p_1 p_2 p_2 \rangle} \right]^{1/(m-1)} \tag{4.1}$$

The critical shear rate for an unfilled system, $\dot{\gamma}_c^{\phi=0}$, is obtained by imposing $\phi = 0$ in (4.1) (see also figure 5). The ratio $\chi = \dot{\gamma}_c^\phi / \dot{\gamma}_c^{\phi=0}$ (or inversely the ratio between the characteristic time for the unfilled and filled systems) is then introduced to investigate the departure from Newtonian behaviour. Hence, if $\chi < 1$, the rod suspension shear thins before the unfilled matrix and the opposite behaviour is observed for $\chi > 1$. Figure 6 depicts the ratio χ as a function of the Péclet number for three different values of the power-law index ($m = 0.9, 0.6$ and 0.3 , respectively).

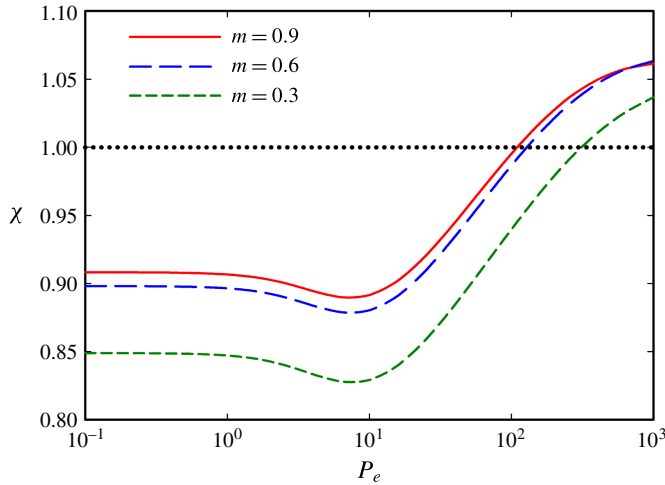


FIGURE 6. (Colour online) χ as a function of P_e for three different values of the power-law index; $m = 0.9, 0.6$ and 0.3 , respectively ($\phi = 10\%$). The dotted line indicates cases when the onset of rod suspension and unfilled matrix shear thinning occur at the same characteristic time.

These results are obtained with $\eta_0 = 1000 \text{ Pa s}$, $\phi = 10\%$ and $K = 1000 \text{ Pa s}^m$ and the dotted line in figure 6 indicates cases when the onset of rod suspension and unfilled matrix shear thinning occur at the same characteristic time. In the following analysis it will be useful to keep in mind the results for rod orientations presented in figure 4. The rod suspension shear thins before the unfilled matrix up to $a_{11}^{(m)} \leq 0.7$ ($P_e \approx 10^2$), otherwise the opposite behaviour is observed and the range within which this phenomenon is noticed increases when decreasing the power-law index. Moreover, the largest departures from $\chi = 1$ appear to match the specific viscosity peaks (see figure 3), where the average rod orientation is the closest to the principal axis of strain ($P_e \approx 10$). As η_0, K and ϕ have been fixed arbitrary, curves plotted in figure 6 cannot be considered as master curves.

4.2. Ellis model

The Ellis model has the advantage of expressing the shear rate as a function of the shear stress. In simple shear flow, the Ellis fluid response can then be written in the following form

$$\frac{\dot{\gamma}}{\tau_{rz}} = \frac{1 + (|\tau_{rz}|/\tau_{1/2})^{\alpha-1}}{\eta_0}. \tag{4.2}$$

This model exhibits a Newtonian fluid character at $\tau_{rz} \rightarrow 0$ (η_0 plateau viscosity) and a non-Newtonian power-law fluid character at high shear rates (α is related to the power-law index by $\alpha = 1/m$). While the index α is a measure of the degree of shear-thinning behaviour (the greater the value of α , the greater is the extent of shear thinning), $\tau_{1/2}$ represents the shear stress value at which the apparent matrix viscosity has dropped to half its zero-shear-rate value (at high shear stress or shear rate, $K = (\eta_0 \tau_{1/2}^{\alpha-1})^{1/\alpha}$). Therefore, the choice of an Ellis fluid appears to be a reasonable compromise as a constitutive model which captures more details of the viscosity

trend observed experimentally. Substituting (4.2) into (2.7) leads to the following expression for the drag force

$$\frac{z}{2} \dot{\gamma} : \mathbf{p}\mathbf{p} = \frac{f}{2\pi\eta_0} \log(h/R) + \frac{f}{2\pi\eta_0} \frac{1}{\alpha - 1} \left(\frac{|f|}{2\pi R\tau_{1/2}} \right)^{\alpha-1} [1 - (R/h)^{\alpha-1}]. \quad (4.3)$$

The drag force f has to be obtained numerically from (4.3) by means of simple numerical solvers based for example on a bi-section method. These do not require high computational time and generally do not restrict the applicability of the model. Hence, after computing the drag force numerically, the rod contribution to the stress tensor components are straightforwardly obtained using (2.8).

The model predictions are analysed by comparing them with experimental data obtained for glass-fibre-reinforced polystyrene melts. The experimental results are taken from the work of Chan *et al.* (1978) and polystyrene (PS) polymers are filled respectively with 0 wt% (PS0), 20 wt% (PS20) and 40 wt% (PS40) of glass fibre of diameter equal to 12.7 μm and length of order 2 mm for the PS20 and 1 mm for the PS40. A nonlinear least-squares algorithm is used to determine the Ellis parameters for the pure PS matrix and the parameters $\eta_0 = 750$ kPa s, $\tau_{1/2} = 120$ kPa and $\alpha = 2.93$ were found. It can be seen in figure 7 that the viscosity of the unfilled polystyrene (PS0) is well predicted for shear rates spanning over six orders of magnitude.

Assuming a polystyrene density of $\rho_{PS} = 1.00$ g cm⁻³ and a glass-fibre density of $\rho_{fib} = 2.50$ g cm⁻³, the calculated volume concentrations are found to be $\phi_{PS20} = 9.1\%$ and $\phi_{PS40} = 21.1\%$ for PS20 and PS40, respectively. The same fitting procedure is applied to obtain the shear viscosities of PS20 and PS40, as shown in figure 7. Note that the rod orientation state is given by the steady-state solution of the Fokker-Planck equation (3.5) (that is a non-isotropic orientation for the distribution function) and, h appearing in (4.3) with P_e are chosen as the two fitting parameters. Due to the important particle length, fibre breakage during the measurements cannot be ruled out and the values of h and P_e remain uncertain. The nonlinear least-squares algorithm gives $h = 14.0$ μm and $P_e = 8.70 \times 10^6$ for PS20 and $h = 7.8$ μm and $P_e = 9.85 \times 10^5$ for PS40. As can be seen in figure 7, the model predictions are in good agreement with the experimental findings. The obtained fitting values for P_e suggest that the rod orientation state is in close to perfect alignment leading to a low contribution to the shear stress. However, as the coupling coefficients are due to the high aspect ratios (i.e. ≈ 160 and 80 for PS20 and PS40, respectively), the short glass fibres contribution to the shear stress cannot be omitted. We speculate that the measurement for the fibre dimensions have been performed before preparing the samples for the rheological tests, leading to lower aspect ratios due to fibre length breakage. Chan *et al.* (1978) also reported the existence of normal stresses for the polystyrene systems but their measurements are not employed in our fitting procedure since the Ellis model predicts no normal stresses in shear flows for the unfilled matrix.

χ can be estimated graphically by noting that $\dot{\gamma}_c^\phi = (\eta_{PS20}^N|_{\dot{\gamma}=0.001\text{s}^{-1}}/\eta_{PS20}^{PL}|_{\dot{\gamma}=1\text{s}^{-1}})^{1/(m-1)}$ and $\dot{\gamma}_c^{\phi=0} = (\eta_{PS0}^N|_{\dot{\gamma}=0.001\text{s}^{-1}}/\eta_{PS0}^{PL}|_{\dot{\gamma}=1\text{s}^{-1}})^{1/(m-1)}$, where $\eta_{PS0}^N|_{\dot{\gamma}=0.001\text{s}^{-1}} \approx 7.5 \times 10^5$ Pa s, $\eta_{PS20}^{PL}|_{\dot{\gamma}=1\text{s}^{-1}} \approx 5.0 \times 10^5$ Pa s, $\eta_{PS0}^N|_{\dot{\gamma}=0.001\text{s}^{-1}} \approx 7.5 \times 10^5$ Pa s and $\eta_{PS0}^{PL}|_{\dot{\gamma}=1\text{s}^{-1}} \approx 2.5 \times 10^5$ Pa s, respectively. Note that $\eta_{PS0}^{PL}|_{\dot{\gamma}=1\text{s}^{-1}}$ and $\eta_{PS20}^{PL}|_{\dot{\gamma}=1\text{s}^{-1}}$ may be obtained by extrapolation of the power-law viscosity curves up to $\dot{\gamma} = 1\text{s}^{-1}$ (in our case, this extrapolation is not necessary). It is then found that $\chi \approx 0.6 < 1$, indicating that the rod suspension shear thins before the unfilled matrix, as also observed experimentally in figure 7.

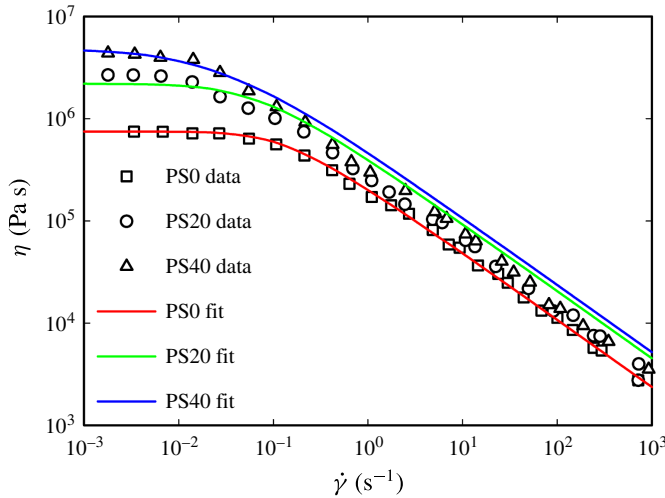


FIGURE 7. (Colour online) Comparison of the steady-shear viscosity for the glass-fibre-filled polystyrene systems (Chan *et al.* 1978) with the model predictions.

4.3. Carreau model

Based on the previous results, we can extend our analysis to rod suspensions in Carreau fluids. By neglecting the viscosity plateau at large shear rates, the Carreau model writes

$$\eta = \eta_0 [1 + (\lambda_0 \dot{\gamma})^2]^{(m-1)/2}, \tag{4.4}$$

where the parameter λ_0 is a time constant for the fluid. The value of λ_0 determines the shear rate at which the transition occurs from the zero-shear-rate plateau to the power-law portion. This time, the micromechanical analysis at the rod scale is numerically performed: equation (2.5) is solved along incremental particle segments to express the shear stress at the wall considering that the fluid follows the Carreau model. Hence, the extra stress due to the particle contribution (2.8) is numerically computed and the material functions for the suspensions can be deduced.

Figure 8 depicts the specific shear viscosities, η_{sp} , when the rods are suspended in a Newtonian, power-law and Carreau fluids, respectively. For the following simulation results, an isotropic rod orientation distribution is assumed ($\psi = 1/4\pi$), the Newtonian viscosity is $\eta_0 = 1000$ Pa s, the consistency is given by $K = \eta_0 \lambda_0^{m-1}$, where the power-law index is $m = 0.3$ and the characteristic time for the Carreau model is $\lambda_0 = 0.1$ s. The particle phase properties are $\phi = 10\%$, $a_r = 20$ and $h = D\sqrt{\pi}/4\phi$. As expected, at low shear rates, the specific viscosity obtained for rods suspended in a Carreau fluid matched the one predicted for a Newtonian suspending fluid (2.15) and at high shear rates, the observed trend is the power-law behaviour (3.3).

This approach to predicting the material functions for rod suspensions in Carreau fluid is useful for viscometric flows but leads to the high computational times required for non-homogenous problems. Although a micromechanical description at the particle scale is of key importance to the understanding of the flow kinematics of suspensions in shear-thinning fluids, the approach used in the case of a Carreau fluid appears to be rather restricted for practical applications, at least for the moment.

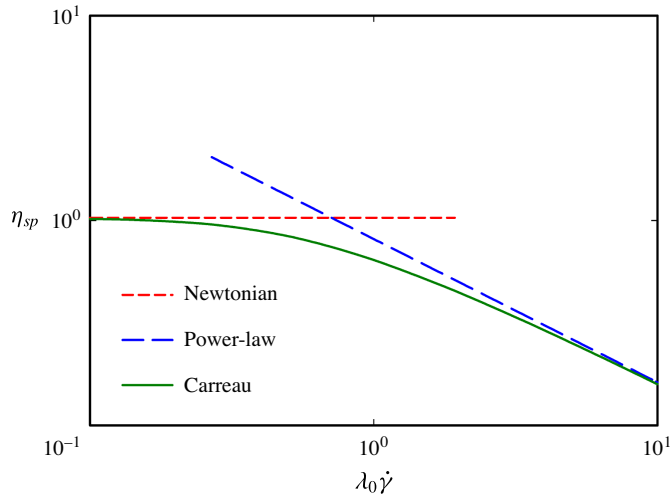


FIGURE 8. (Colour online) Specific viscosities for rod suspensions in Newtonian, power-law and Carreau fluids, respectively.

5. Concluding remarks

In this paper, the cell model (or the self-consistent scheme) is revisited to derive constitutive equations for rod suspensions in non-Newtonian viscous fluids such as power-law, Ellis and Carreau models. The motion of particles in these generalized Newtonian fluids is discussed and it is proposed that the Jeffery solution, developed for Newtonian fluids, can be applied.

The effect of the shear-thinning behaviour of the suspending matrix on rod suspensions is investigated and it appears to be similar to a stretching force on the orientation distribution in the vorticity direction in simple shear flow. Moreover, at a random rod orientation state, the specific shear viscosity for a suspension in a Newtonian fluid is larger than the one in a power-law matrix but the opposite behaviour is observed when most rods have a perfect alignment. It is also found that the departure for rod suspensions from the Newtonian plateau behaviour as compared to the unfilled matrix is dependent on the particle orientation: for rods aligned close to the shear flow direction, the unfilled matrix begins to shear thin before the suspensions. For the other orientation states (i.e. isotropic orientation or rod orientation coincident with the principal axis of strain), the opposite behaviour is observed. While this does not answer why the suspensions of aligned particle shear thin later than the pure matrix, it can be speculated that non-aligned particles create more disturbance in the flow field and hence generate higher local velocity gradients, which in turn lead to earlier shear thinning.

A semi-analytical model for rod suspensions in Ellis fluid is also proposed and the results obtained suggest that this approach is suitable for predicting a Newtonian plateau at lower shear rates and a shear-thinning behaviour at high shear rates. The good agreement between model predictions and experimental data for the shear viscosities of glass-fibre-filled polystyrene melts (Chan *et al.* 1978) increases our confidence in the proposed method. Finally, a micromechanical analysis is performed at the particle scale by considering a Carreau fluid in order to predict some material properties of the rod suspension but this strategy requires higher computational time, especially in the case of suspensions in general flow fields.

Although extensional flows are not investigated in this paper, and hence the effect of strain-thinning behaviour on rod suspensions has not been considered, we expect our approach to be valid in such flows as it is based on the works of Batchelor (1971) and Goddard (1976a,b): the former considered the stress generated in a non-dilute suspension of rods by pure straining motion for Newtonian fluids while the latter studied the tensile stress contribution of rods in power-law fluids, both of them assumed the slender particles to be aligned parallel to the direction of the greatest principal rate of extension.

Acknowledgements

This work has been performed while J.F. was on sabbatical leave at the National University of Singapore (NUS), as visitor Professor at the Department of Mechanical Engineering. J.F. wishes to thank his hosts Professor N. Phan-Thien and Professor B. C. Khoo for their kind hospitality and a very stimulating environment. The authors are grateful to the reviewers for their useful and significant suggestions.

Appendix A. Derivation of the time evolution equation for $\langle |\dot{\gamma} : pp|^{m-1} pp \rangle$

The equation of change for $\langle \mathbf{B} \rangle$, where $\mathbf{B} = |\dot{\gamma} : pp|^{m-1} pp$ is a symmetric second-order tensor function of \mathbf{p} , $\dot{\gamma}$ and m , is derived. Equation (3.5) is then multiplied by \mathbf{B} and integrated over all possible directions of \mathbf{p} to give

$$\int_p \frac{D\psi}{Dt} \mathbf{B} \, d\mathbf{p} = - \int_p \frac{\partial}{\partial \mathbf{p}} \cdot (\dot{\mathbf{p}} \psi) \mathbf{B} \, d\mathbf{p} + \int_p C_I |\dot{\gamma}| \frac{\partial^2 \psi}{\partial p^2} \mathbf{B} \, d\mathbf{p}. \tag{A 1}$$

Equation (A 1) involves a convective term (the first term on the right-hand side) and a diffusive term proportional to $C_I |\dot{\gamma}|$. Since $\dot{\gamma}$ and m are assumed to be time independent and \mathbf{B} is a function of \mathbf{p} , the left-hand side can be rewritten as

$$\int_p \frac{D\psi}{Dt} \mathbf{B} \, d\mathbf{p} = \frac{D}{Dt} \langle \mathbf{B} \rangle. \tag{A 2}$$

The term on the right-hand side of (A 1) is then expanded using integration by parts with the assumption that $C_I |\dot{\gamma}|$ is not a function of \mathbf{p} , this yields

$$\frac{D\langle \mathbf{B} \rangle}{Dt} = \int_p \dot{\mathbf{p}} \cdot \frac{\partial \mathbf{B}}{\partial \mathbf{p}} \psi \, d\mathbf{p} - C_I |\dot{\gamma}| \int_p \frac{\partial \psi}{\partial \mathbf{p}} \cdot \frac{\partial \mathbf{B}}{\partial \mathbf{p}} \, d\mathbf{p}. \tag{A 3}$$

The second term on the right-hand side is again expanded using integration by parts (Advani & Tucker 1987) resulting in

$$\frac{D\langle \mathbf{B} \rangle}{Dt} = \left\langle \dot{\mathbf{p}} \cdot \frac{\partial \mathbf{B}}{\partial \mathbf{p}} \right\rangle + C_I |\dot{\gamma}| \left\langle \frac{\partial \mathbf{B}^2}{\partial p^2} \right\rangle. \tag{A 4}$$

If the Jeffery equation for slender bodies is substituted into (A 4), the first term on the right-hand side of (A 4) becomes, when \mathbf{B} is replaced by $|\dot{\gamma} : pp|^{m-1} pp$:

$$\left\langle \dot{\mathbf{p}} \cdot \frac{\partial}{\partial \mathbf{p}} (|\dot{\gamma} : pp|^{m-1} pp) \right\rangle = \left\langle |\dot{\gamma} : pp|^{m-1} \dot{\mathbf{p}} \cdot \frac{\partial}{\partial \mathbf{p}} (pp) \right\rangle + \left\langle \dot{\mathbf{p}} \cdot pp \frac{\partial}{\partial \mathbf{p}} (|\dot{\gamma} : pp|^{m-1}) \right\rangle. \tag{A 5}$$

Bird *et al.* (1987*b*) show that $\partial/\partial\mathbf{p}(\mathbf{p}\mathbf{p}) = (\boldsymbol{\delta} - \mathbf{p}\mathbf{p})\mathbf{p} + [\mathbf{p}(\boldsymbol{\delta} - \mathbf{p}\mathbf{p})]^t$ and by noting that $\dot{\mathbf{p}} \cdot \mathbf{p} = 0$ (the inextensibility condition), equation (A 5) results in

$$\begin{aligned} \left\langle \dot{\mathbf{p}} \cdot \frac{\partial}{\partial \mathbf{p}} (|\dot{\boldsymbol{\gamma}} : \mathbf{p}\mathbf{p}|^{m-1} \mathbf{p}\mathbf{p}) \right\rangle &= -\frac{1}{2}(\boldsymbol{\omega} \cdot \langle |\dot{\boldsymbol{\gamma}} : \mathbf{p}\mathbf{p}|^{m-1} \mathbf{p}\mathbf{p} \rangle - \langle |\dot{\boldsymbol{\gamma}} : \mathbf{p}\mathbf{p}|^{m-1} \mathbf{p}\mathbf{p} \rangle \cdot \boldsymbol{\omega}) \\ &\quad + \frac{1}{2}(\dot{\boldsymbol{\gamma}} \cdot \langle |\dot{\boldsymbol{\gamma}} : \mathbf{p}\mathbf{p}|^{m-1} \mathbf{p}\mathbf{p} \rangle + \langle |\dot{\boldsymbol{\gamma}} : \mathbf{p}\mathbf{p}|^{m-1} \mathbf{p}\mathbf{p} \rangle \cdot \dot{\boldsymbol{\gamma}} \\ &\quad - 2\dot{\boldsymbol{\gamma}} : \langle |\dot{\boldsymbol{\gamma}} : \mathbf{p}\mathbf{p}|^{m-1} \mathbf{p}\mathbf{p}\mathbf{p}\mathbf{p} \rangle). \end{aligned} \quad (\text{A } 6)$$

Therefore, the convective part of equation (A 4) reads

$$\begin{aligned} \frac{D\langle |\dot{\boldsymbol{\gamma}} : \mathbf{p}\mathbf{p}|^{m-1} \mathbf{p}\mathbf{p} \rangle}{Dt} &= -\frac{1}{2}(\boldsymbol{\omega} \cdot \langle |\dot{\boldsymbol{\gamma}} : \mathbf{p}\mathbf{p}|^{m-1} \mathbf{p}\mathbf{p} \rangle - \langle |\dot{\boldsymbol{\gamma}} : \mathbf{p}\mathbf{p}|^{m-1} \mathbf{p}\mathbf{p} \rangle \cdot \boldsymbol{\omega}) \\ &\quad + \frac{1}{2}(\dot{\boldsymbol{\gamma}} \cdot \langle |\dot{\boldsymbol{\gamma}} : \mathbf{p}\mathbf{p}|^{m-1} \mathbf{p}\mathbf{p} \rangle + \langle |\dot{\boldsymbol{\gamma}} : \mathbf{p}\mathbf{p}|^{m-1} \mathbf{p}\mathbf{p} \rangle \cdot \dot{\boldsymbol{\gamma}} \\ &\quad - 2\dot{\boldsymbol{\gamma}} : \langle |\dot{\boldsymbol{\gamma}} : \mathbf{p}\mathbf{p}|^{m-1} \mathbf{p}\mathbf{p}\mathbf{p}\mathbf{p} \rangle), \end{aligned} \quad (\text{A } 7)$$

which is precisely equation (3.4). Unfortunately, we are not able to derive a simple expression for the diffusion part.

REFERENCES

- ADVANI, S. G. & TUCKER, C. L. 1987 The use of tensors to describe and predict fiber orientation in short fiber composites. *J. Rheol.* **31** (8), 751–784.
- ADVANI, S. G. & TUCKER, C. L. 1990 Closure approximations for three-dimensional structure tensors. *J. Rheol.* **34** (3), 367–386.
- AIT-KADI, A. & GRMELA, M. 1994 Modelling the rheological behaviour of fibre suspensions in viscoelastic media. *J. Non-Newtonian Fluid Mech.* **53**, 65–81.
- AZAEZ, J. 1996 Constitutive equations for fiber suspensions in viscoelastic media. *J. Non-Newtonian Fluid Mech.* **66** (1), 35–54.
- BATCHELOR, G. K. 1971 The stress generated in a non-dilute suspension of elongated particles by pure straining motion. *J. Fluid Mech.* **46** (4), 813–829.
- BAY, R. S. 1991 Fiber orientation in injection-molded composites: a comparison of theory and experiment. PhD dissertation.
- BEAULNE, M. & MITSOULIS, E. 2003 Rheological characterization of fiber-filled polymer composites via constitutive modeling. *J. Reinforced Plastics Compos.* **22** (17), 1625–1640.
- BECRAFT, M. L. & METZNER, A. B. 1992 The rheology, fiber orientation, and processing behavior of fiber filled fluids. *J. Rheol.* **36** (1), 143–174.
- BIRD, R. B., ARMSTRONG, R. C. & HASSAGER, O. 1987*a* *Dynamics of Polymeric Liquids. Fluid Mechanics*, 2nd edn. vol. 1. Wiley.
- BIRD, R. B., CURTISS, C. F., ARMSTRONG, R. C. & HASSAGER, O. 1987*b* *Dynamics of Polymeric Liquids. Kinetic Theory*, 2nd edn. vol. 2. Wiley.
- CHAN, Y., WHITE, J. L. & OYANAGI, Y. 1978 A fundamental study of the rheological properties of glass-fiber-reinforced polyethylene and polystyrene melts. *J. Rheol.* **22** (5), 507–524.
- CHUNG, S. T. & KWON, T. H. 1996 Coupled analysis of injection molding filling and fiber orientation, including in-plane velocity gradient effect. *Polym. Compos.* **17** (6), 859–872.
- CINTRA, J. S. & TUCKER, C. L. 1995 Orthotropic closure approximations for flow-induced fiber orientation. *J. Rheol.* **39** (6), 1095–1122.
- CZARNECKI, L. & WHITE, J. L. 1980 Shear flow rheological properties, fiber damage, and mastication characteristics of aramid-, glass-, and cellulose-fiber-reinforced polystyrene melts. *J. Appl. Polym. Sci.* **25** (6), 1217–1244.

- DINH, S. M. & ARMSTRONG, R. C. 1984 A rheological equation of state for semiconcentrated fiber suspensions. *J. Rheol.* **28** (3), 207–227.
- DOI, M. & EDWARDS, S. F. 1986 *The Theory of Polymer Dynamics*. Oxford Science Publications.
- DUPRET, F. & VERLEYE, V. 1999 *Modeling the Flow of Fiber Suspensions in Narrow Gaps*, 8th edn. vol. 2, pp. 19–29. Elsevier.
- FÉREC, J. & AUSIAS, G. 2015 *Rheological Modeling of Non-dilute Rod Suspensions*, pp. 77–118. Wiley.
- FÉREC, J., HENICHE, M., HEUZEY, M. C., AUSIAS, G. & CARREAU, P. J. 2008 Numerical solution of the Fokker–Planck equation for fiber suspensions: application to the Folgar–Tucker–Lipscomb model. *J. Non-Newtonian Fluid Mech.* **155** (12), 20–29.
- FÉREC, J., HEUZEY, M.-C., PÉREZ-GONZÁLEZ, J., VARGAS, L., AUSIAS, G. & CARREAU, P. J. 2009 Investigation of the rheological properties of short glass fiber-filled polypropylene in extensional flow. *Rheol. Acta* **48** (1), 59–72.
- FOLGAR, F. & TUCKER, C. L. 1984 Orientation behavior of fibers in concentrated suspensions. *J. Reinforced Plastics Compos.* **3** (2), 98–119.
- GIBSON, A. G. & TOLL, S. 1999 Mechanics of the squeeze flow of planar fibre suspensions. *J. Non-Newtonian Fluid Mech.* **82**, 1–24.
- GIESEKUS, H. 1962 Elasto-viskose Flüssigkeiten, für die in stationären schichtströmungen sämtliche normalspannungskomponenten verschieden groß sind. *Rheol. Acta* **2** (01), 50–62.
- GODDARD, J. D. 1976a The stress field of slender particles oriented by a non-Newtonian extensional flow. *J. Fluid Mech.* **78** (1), 177–206.
- GODDARD, J. D. 1976b Tensile stress contribution of flow-oriented slender particles in non-Newtonian fluids. *J. Non-Newtonian Fluid Mech.* **1** (1), 1–17.
- GODDARD, J. D. 1978 Tensile behavior of powerlaw fluids containing oriented slender fibers. *J. Rheol.* **22** (6), 615–622.
- GREENE, J. P. & WILKES, J. O. 1995 Steady-state and dynamic properties of concentrated fiber-filled thermoplastics. *Polym. Engng Sci.* **35** (21), 1670–1681.
- HINCH, E. J. & LEAL, L. G. 1975 Constitutive equations in suspension mechanics. Part 1. General formulation. *J. Fluid Mech.* **71** (3), 481–495.
- JEFFERY, G. B. 1922 The motion of ellipsoidal particles immersed in a viscous fluid. *Proc. R. Soc. Lond.* **102**, 161–179.
- KAGARISE, C., MIYAZONO, K., MAHBOOB, M., KOELLING, K. W. & BECHTEL, S. E. 2011 A constitutive model for characterization of shear and extensional rheology and flow induced orientation of carbon nanofiber/polystyrene melt composites. *J. Rheol.* **55** (4), 781–807.
- KAGARISE, C., XU, J., WANG, Y., MAHBOOB, M., KOELLING, K. W. & BECHTEL, S. E. 2010 Transient shear rheology of carbon nanofiber/polystyrene melt composites. *J. Non-Newtonian Fluid Mech.* **165** (34), 98–109.
- KITANO, T. & KATAOKA, T. 1980 The effect of the mixing methods on viscous properties of polyethylene melts filled with fibers. *Rheol. Acta* **19** (6), 753–763.
- KITANO, T., KATAOKA, T. & NAGATSUKA, Y. 1984 Shear flow rheological properties of vinylon- and glass-fiber reinforced polyethylene melts. *Rheol. Acta* **23** (1), 20–30.
- MOBUCHON, C., CARREAU, P. J., HEUZEY, M.-C., SEPEHR, M. & AUSIAS, G. 2005 Shear and extensional properties of short glass fiber reinforced polypropylene. *Polym. Compos.* **26** (3), 247–264.
- NISHITANI, Y., SEKIGUCHI, I., HAUSNEROVA, B., ZDRAZILOVA, N. & KITANO, T. 2007 Rheological properties of aminosilane surface treated short glass fibre reinforced polypropylenes. Part 1: steady shear and oscillatory flow properties in molten state. *Polymer Polym. Compos.* **15** (2), 111–119.
- OUARI, N., KACI, A., TAHAKOURT, A. & CHAOUICHE, M. 2011 Rheological behaviour of fibre suspensions in non-Newtonian fluids. *Appl. Rheol.* **21** (5), 54801.
- PHAN-THIEN, N., FAN, X. J., TANNER, R. I. & ZHENG, R. 2002 Folgar–Tucker constant for a fibre suspension in a Newtonian fluid. *J. Non-Newtonian Fluid Mech.* **103** (2–3), 251–260.
- POSLINSKI, A. J., RYAN, M. E., GUPTA, R. K., SESHADRI, S. G. & FRECHETTE, F. J. 1988 Rheological behavior of filled polymeric systems I. Yield stress and shearthinning effects. *J. Rheol.* **32** (7), 703–735.

- RAJABIAN, M., DUBOIS, C. & GRMELA, M. 2005 Suspensions of semiflexible fibers in polymeric fluids: rheology and thermodynamics. *Rheol. Acta* **44** (5), 521–535.
- RAMAZANI, S. A., AIT-KADI, A. & GRMELA, M. 1997 Rheological modelling of short fiber thermoplastic composites. *J. Non-Newtonian Fluid Mech.* **73** (3), 241–260.
- RAMAZANI, S. A., AIT-KADI, A. & GRMELA, M. 2001 Rheology of fiber suspensions in viscoelastic media: experiments and model predictions. *J. Rheol.* **45** (4), 945–962.
- SEPEHR, M., CARREAU, P. J., GRMELA, M., AUSIAS, G. & LAFLEUR, P. G. 2004 Comparison of rheological properties of fiber suspensions with model predictions. *J. Polym. Engng* **24** (6), 579–610.
- SOULOUMIAC, B. & VINCENT, M. 1998 Steady shear viscosity of short fibre suspensions in thermoplastics. *Rheol. Acta* **37** (3), 289–298.
- WANG, M. L. & CHEAU, T. C. 1991 A constitutive approach for studying concentrated suspensions of rigid fibers in a non-Newtonian Ellis fluid. *J. Chin. Inst. Engng* **14** (5), 483–493.
- WHITE, J. L. & CZARNECKI, L. 1980 Notes: on papers by Chan, White, and Oyanagi and by Goddard on elongational flow behavior of fiber-reinforced polymer melts. *J. Rheol.* **24** (4), 501–506.